Assembly of Bimetallic Gold−Silver Nanoparticles via Selective Interparticle Dicarboxylate−Silver Linkages

Nancy N. Kariuki, Jin Luo, Syed A. Hassan, I.-Im S. Lim, Lingyan Wang, and Chuan Jian Zhong*

Department of Chemistry, State University of New York at Binghamton, Binghamton, New York 13902

Received August 29, 2005. Revised Manuscript Received October 28, 2005

This article describes findings of an investigation of the thin-film assembly of binary metal nanoparticles via interparticle linkages of dicarboxylic acid mediators at selective metal sites. Decanethiol- (DT-) capped gold−silver (Au−Ag) alloy nanoparticles of ∼3-nm core sizes were chosen as a model system because of the unique carboxylate−Ag^+ binding chemistry and the well-defined thiolate-capping capability at Au. The dicarboxylate-mediated thin-film assembly of Au−Ag nanoparticles was characterized using UV−vis, TEM, XPS, FTIR, and NMR techniques. The results from controlling the oxidative or reductive conditions reveal that the oxidation of Ag to Ag^+ on the alloy nanocrystal surface played an important role in the selective ligand exchange and interparticle linkage by dicarboxylic acids (e.g., hexadecanedioic acid, HDA). The formation of the thin-film assembly is dependent on both the alloy composition of the Au−Ag nanoparticles and the chain length of the dicarboxylic acids. The degree for an HDA−DT/Au−Ag exchanging and linking system is determined to yield a value of 16% of DTs per Au−Ag particle being displaced by HDAs. In comparison to similar thin-film assemblies of Au−Ag and Au nanoparticles by other mediators, the results support the conclusion that the HDA-mediated assembly of Au−Ag nanoparticles occurs via $-CO_2^--Ag^+$ linkages at silver sites forming a mediator (HDA)−template (DT) nanostructure. The nanostructured thin-film assemblies exhibit interesting optical and electronic properties, which have important implications for the exploration of binary nanoparticle-structured materials for sensing and catalytic applications where fine-tuning of either the binary nanocrystal cores or the bifunctional interparticle structures is desired.

Introduction

The ability to assemble nanoparticles with defined interparticle spatial and chemical properties is critical to the exploration of the nanoparticle-structured electronic, optical, magnetic, catalytic, and chemical or biological properties.[1,2] A number of approaches have been demonstrated for the synthesis and assembly of metal nanoparticles. Examples include two-phase synthesis of monolayer-protected nanoparticles,[3−8] stepwise layer-by-layer construction,[9−12] DNA complimentary binding,[13−15] polymer or dendrimer mediated assemblies,[16−19] and mediator−template assem-

* To whom correspondence should be addressed. Phone: 607-777-4605. E-mail: cjzhong@binghamton.edu.

(1) Daniel, M. C.; Astruc, D. *Chem. Rev.* **2004**, *104*, 293.
(2) Templeton, A. C.; Murray, R. W. *Acc. Chem. Res.* **2000**, *33*, 27 and references therein.
(3) (a) Brust, M.; Bethell, D.; Kiely, C. J.; Schiffrin, D. J. *Langmuir* **1998**, *14*, 5425. (b) Gittins, D. I.; Bethell, D.; Schiffrin, D. J.; Nichols, R. J. *Nature* **2000**, *408*, 67.
(4) (a) Lahtinen, R. M.; Mertens, S. F. L.; East, E.; Kiely, C. J.; Schiffrin, D. J. *Langmuir* **2004**, *20*, 3289. (b) Brust, M.; Walker, M.; Bethell, D.; Schiffrin, D. J.; Whyman, R. *J. Chem. Soc., Chem. Commun.* **1994**, 801.
(5) (a) Hostetler, M. J.; Wingate, J. E.; Zhong, C. J.; Harris, J. E.; Vachet, R. W.; Clark, M. R.; Londono, J. D.; Green, S. J.; Stokes, J. J.; Wignall, G. D.; Glish, G. L.; Porter, M. D.; Evans, N. D.; Murray, R. W. *Langmuir* **1998**, *14*, 17. (b) Hostetler, M. J.; Zhong, C. J.; Yen, B. K. H.; Anderegg, J.; Gross, S. M.; Evans, N. D.; Porter, M. D.; Murray, R. W. *J. Am. Chem. Soc.* **1998**, *120*, 9396.
(6) Kariuki, N. N.; Luo, J.; Maye, M. M.; Hassan, A.; Menard, T.; Naslund, H. R.; Lin, Y.; Wang, C.; Engelhard, M. H.; Zhong, C. J. *Langmuir* **2004**, *20*, 11240.
(7) Mallin, M. P.; Murphy, C. J. *Nano Lett.* **2002**, *2*, 1235.
(8) Rodriguez-Gonzalez, B.; Sanchez-Iglesias, A.; Giersig, M.; Liz-Marzan, L. M. *Faraday Discuss.* **2004**, *125*, 133.
(9) (a) Wang, Z. L. *Adv. Mater.* **1998**, *10*, 13. (b) Whetten, R. L.; Khoury, J. T.; Alvarez, M. M.; Murthy, S.; Vezmar, I.; Wang, Z. L.; Stephens, P. W.; Cleveland, C. L.; Luedtke, W. D.; Landman, U. *Adv. Mater.* **1996**, *8*, 428. (c) Wang, Z. L.; Harfenist, S. A.; Vezmar, I.; Whetten, R. L.; Bentley, I.; Evans, N. D.; Alexander, K. B. *Adv. Mater.* **1998**, *10*, 808.
(10) (a) Bethell, D.; Brust, M.; Schiffrin, D. J.; Kiely, C. *J. Electroanal. Chem.* **1996**, *409*, 137. (b) Brust, M.; Kiely, C. J.; Bethell, D.; Schiffrin, D. J. *J. Am. Chem. Soc.* **1998**, *120*, 12367. (c) Baum, T.; Bethell, D.; Brust, M.; Schiffrin, D. J. *Langmuir* **1985**, *1*, 866.
(11) (a) Musick, M. D.; Pena, D. J.; Botsko, S. L.; McEvoy, T. M.; Richardson, J. N.; Natan, M. J. *Langmuir* **1999**, *15*, 844. (b) Keating, C. D.; Musick, M. D.; Lyon, L. A.; Brown, K. R.; Baker, B. E.; Pena, D. J.; Feldheim, D. L.; Mallouk, T. E.; Natan, M. J. *ACS Symp. Ser.* **1997**, *679*, 7.
(12) (a) Zamborini, F. P.; Hicks, J. F.; Murray, R. W. *J. Am. Chem. Soc.* **2000**, *122*, 4514. (b) Templeton, A. C.; Zamborini, F. P.; Wuelfing, W. P.; Murray, R. W. *Langmuir* **2000**, *16*, 6682. (c) Wuelfing, W. P.; Zamborini, F. P.; Templeton, A. C.; Wen, X. G.; Yoon, H.; Murray, R. W. *Chem. Mater.* **2001**, *13*, 87.
(13) (a) Mirkin, C. A.; Letsinger, R. L.; Mucic, R. C.; Storhoff, J. J. *Nature* **1996**, *382*, 607. (b) Elghanian, R.; Storhoff, J. J.; Mucic, R. C.; Letsinger, R. L.; Mirkin, C. A. *Science* **1997**, *277*, 1078. (c) Taton, T. A.; Mucic, R. C.; Mirkin, C. A.; Letsinger, R. L. *J. Am. Chem. Soc.* **2000**, *122*, 6305. (d) Storhoff, J. J.; Lazarides, A. A.; Mucic, R. C.; Mirkin, C. A.; Letsinger, R. L.; Schatz, G. C. *J. Am. Chem. Soc.* **2000**, *122*, 4640.
(14) (a) Bruchez, M.; Moronne, M.; Gin, P.; Weiss, S.; Alivisatos, A. P. *Science* **1998**, *281*, 2013. (b) Alivisatos, A. P.; Johnsson, K. P.; Peng, X. G.; Wilson, T. E.; Loweth, C. J.; Bruchez, M. P.; Schultz, P. G. *Nature* **1996**, *382*, 609.
(15) Mbindyo, J. K. N.; Reiss, B. D.; Martin, B. R.; Keating, C. D.; Natan, M. J.; Mallouk, T. E. *Adv. Mater.* **2001**, *13*, 249.
(16) Kariuki, N. N.; Han, L.; Ly, N. K.; Patterson, M. J.; Maye, M. M.; Liu, G. J.; Zhong, C. J. *Langmuir* **2002**, *18*, 8255.

10.1021/cm0519479 CCC: $33.50
Published on Web 12/01/2005

Scheme 1. Schematic Illustrations of Surface Binding Sites and the Selective Linkage for the Assembly of Binary Metal Nanoparticles (e.g., Au−Ag) Mediated by Dicarboxylic Acid

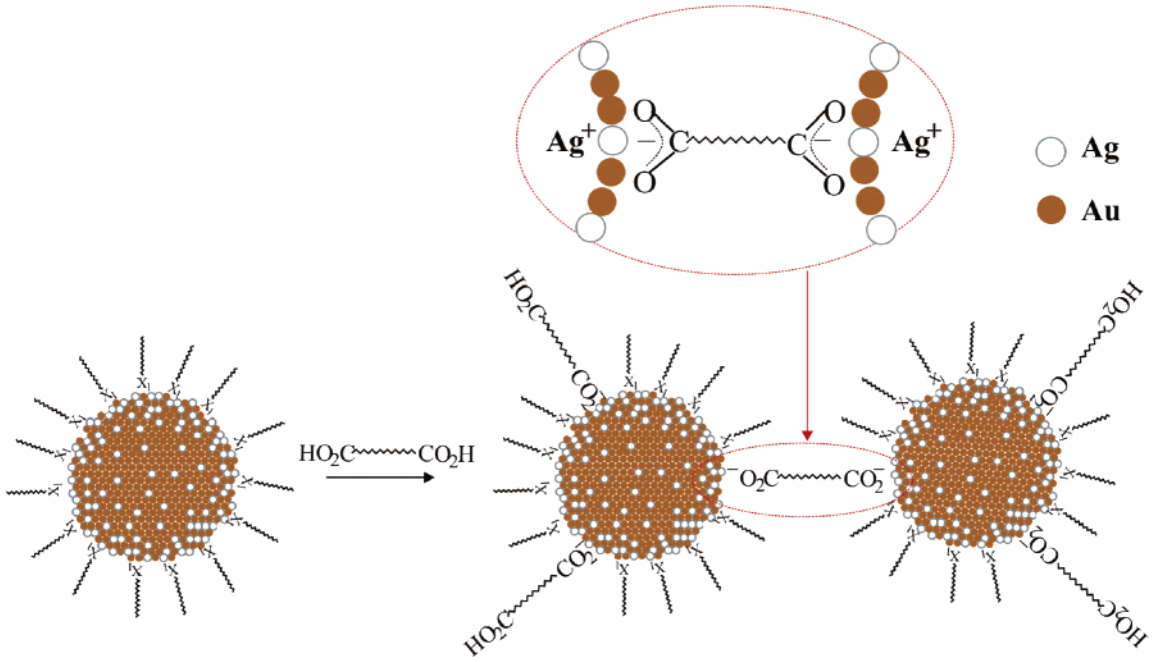

blies.[20] The study of bimetallic or trimetallic nanoparticles has attracted increasing interest because of their interesting optical,[21,22] magnetic,[23,24] and catalytic properties.[25−31] One example involves gold−silver alloy nanoparticles of variable composition in manipulating colors and surface plasmon resonance bands.[6,7] The composition of the bimetallic nanocrystals can alter the wavelength of the optical properties. Another example involves the manipulation of the magnetic properties as a result of the formation of Pt−Fe alloy nanoparticles.[23] It has been demonstrated that an assembly of magnetic nanocrystals as small as 4 nm can support stable magnetization-reversal transitions at room temperature. Recently, gold-based bimetallic nanoparticles are emerging as potential catalysts for fuel-cell reactions.[25−31] An example is the use of gold−platinum alloys as electrocatalysts for methanol oxidation[29] and oxygen reduction[30] reactions. The use of bimetallic nanoparticles for bioanalytical and biomedical probes[32] has also been reported. In these examples, an understanding of the nanoparticle assembly and the interparticle interactions is very important. Whereas the synthesis and assembly of monometallic nanoparticles (e.g., gold) has been studied extensively,[3−20] little is known about the assembly of binary or ternary metal nanoparticle systems, which is in part due to the lack of controllability over the interparticle linkages at the multicomponent nanocrystal surfaces.

In this report, we describe a novel strategy toward the assembly of bimetallic nanoparticles via interparticle linkages of mediator/linker molecules at selective surface metal sites (Scheme 1). Gold−silver (Au−Ag) alloy nanoparticles with ∼3-nm core sizes were chosen as a model system because of the unique carboxylate−Ag^+ binding chemistry at silver

(17) (a) Boal, A. K.; Rotello, V. M. *J. Am. Chem. Soc.* **1999**, *121*, 4914. (b) Boal, A. K.; Rotello, V. M. *Langmuir* **2000**, *16*, 9527. (c) Lahav, M.; Shipway, A. N.; Willner, I. *J. Chem. Soc., Perkin Trans.* **1999**, *2*, 1925. (d) Chen, S. W.; Pei, R. J. *J. Am. Chem. Soc.* **2001**, *123*, 10607. (e) Kim, B.; Tripp, S. L.; Wei, A. *J. Am. Chem. Soc.* **2001**, *123*, 7955.
(18) (a) Shon, Y.-S.; Choo, H. *Chem. Commun.* **2002**, 2560. (b) Guldi, D. M.; Zilbermann, I.; Anderson, G.; Kotov, N. A.; Tagmatarchis, N.; Prato, M. *J. Am. Chem. Soc.* **2004**, *126*, 14340.
(19) (a) Boal, A. K.; Ilhan, F.; DeRouchey, J. E.; Thurn-Albrecht, T.; Russell, T. P.; Rotello, V. M. *Nature* **2000**, *404*, 746. (b) Srivastava, S.; Frankamp, B. L.; Rotello, V. M. *Chem. Mater.* **2005**, *17*, 487.
(20) (a) Zheng, W. X.; Maye, M. M.; Leibowitz, F. L.; Zhong, C. J. *Anal. Chem.* **2000**, *72*, 2190. (b) Han, L.; Maye, M. M.; Leibowitz, F. L.; Ly, N. K.; Zhong, C. J. *J. Mater. Chem.* **2001**, *11*, 1258. (c) Han, L.; Daniel, D. R.; Maye, M. M.; Zhong, C. J. *Anal. Chem.* **2001**, *73*, 4441. (d) Lim, I.-I. S.; Maye, M. M.; Luo, J.; Zhong, C. J. *J. Phys. Chem. B* **2005**, *109*, 2578. (e) Leibowitz, F. L.; Zheng, W. X.; Maye, M. M.; Zhong, C. J. *Anal. Chem.* **1999**, *71*, 5076.
(21) (a) Sinzig, J.; Radtke, U.; Quinten, M.; Kreibig, U. *Z. Phys. D* **1993**, *26*, 242. (b) Toshima, N.; Harada, M.; Yamazaki, Y.; Asakura, K. *J. Phys. Chem.* **1992**, *96*, 9927. (c) Remita, S.; Mostafavi, M.; Delcourt, M. O. *Radiat. Phys. Chem.* **1996**, *47*, 275. (d) Liz-Marzan, L. M.; Philipse, A. P. *J. Phys. Chem.* **1995**, *99*, 15120. (e) Remita, H.; Khatouri, J.; Treguer, M.; Amblard, J.; Belloni, J. *Z. Phys. D* **1997**, *40*, 127. (f) Stroyuk, A. L.; Shvalagin, V. V.; Kuchmii, S. Y. *J. Photochem. Photobiol. A: Chem.* **2005**, *173* 185.
(22) (a) Rodriguez-Gonzalez, B.; Burrows, A.; Watanabe, M.; Kiely, C. J.; Liz-Marzan, L. M. *J. Mater. Chem.* **2005**, *15*, 1759. (b) Rodriguez-Gonzalez, B.; Sanchez-Iglesias, A.; Giersig, M.; Liz-Marzan, L. M. *Faraday Discuss.* **2004**, *125*, 133.
(23) (a) Sun, S. H.; Murray, C. B.; Weller, D.; Folks, L.; Moser, A. *Science* **2000**, *287*, 1989. (b) Sun, S. H.; Fullerton, E. E.; Weller, D.; Murray, C. B. *IEEE Trans. Magn.* **2001**, *37*, 1239.
(24) Chen, M.; Nikles, D. E. *Nano Lett.* **2002**, *2*, 211.
(25) Lu, G. Q.; Wieckowski, A. *Curr. Opin. Colloid Interface Sci.* **2000**, *5*, 95.
(26) Roucoux, A.; Schulz, J.; Patin, H. *Chem. Rev.* **2002**, *102*, 3757.
(27) Long, J. W.; Stroud, R. M.; Swider-Lyons, K. E.; Rolison, D. R. *J. Phys. Chem. B* **2000**, *104*, 9772.
(28) Ley, K. L.; Liu, R. X.; Pu, C.; Fan, Q. B.; Leyarovska, N.; Segre, C.; Smotkin, E. S. *J. Electrochem. Soc.* **1997**, *144*, 1543.
(29) Luo, J.; Maye, M. M.; Kariuki, N. N.; Wang, L.; Njoki, P.; Han, L.; Schadt, M.; Lin, Y.; Naslund, H. R.; Zhong, C. J. *Catal. Today* **2005**, *99*, 291.
(30) Maye, M. M.; Kariuki, N. N.; Luo, J.; Han, L.; Njoki, P.; Wang, L.; Lin, Y.; Naslund, H. R.; Zhong, C. J. *Gold Bull.* **2004**, *37*, 217.
(31) Zhong, C. J.; Luo, J.; Maye, M. M.; Han, L.; Kariuki, N. N. Nanostructured Gold and Alloy Electrocatalysts. In *Nanotechnology in Catalysis*; Zhou, B., Hermans, S., Somorjai, G. A., Eds.; Kluwer Academic/Plenum Publishers, 2004; Vol. 1., Chapter 11, pp 222−248.
(32) (a) Salem, A. K.; Searson, P. C.; Leong, K. W. *Nat. Mater.* **2003**, *2*, 668. (b) Dumitrascu, G.; Kumbhar, A.; Zhou, W. L.; Rosenzweig, Z. *IEEE Trans. Magn.* **2001**, *37*, 2932.

and the well-defined thiolate-capping capability at gold. This strategy explores the combination of gold−sulfur affinity[33,34] and silver−carboxylate[35,36] binding via selective interparticle linkages at the silver sites for the assembly of Au−Ag nanoparticles. The dicarboxylate linking agent has a strong affinity to Ag^+ sites, whereas the alkanethiolates function as a templating agent through strong chain−chain van der Waals interactions; both of these features have been documented by extensive studies of self-assembled monolayers of thiols and alkanoic acids on gold or silver surfaces.[33−36] We demonstrate here for the first time that the dicarboxylate−silver linkage is viable for the assembly of Au−Ag nanoparticles into thin films. An important attribute for the demonstration of the selective interparticle linkage in a mediator−template pathway is the viability of manipulating the bimetallic core composition.[5−8,22]

Experimental Section

Chemicals. Tetrachlorohydrogenaurate trihydrate ($HAuCl_4 \cdot 3H_2O$, 99%), silver nitrate ($AgNO_3$, >99%), potassium bromide (KBr, >99%), tetraoctylammonium bromide (TOABr, 99%), decanethiol (DT, 96%), 1,9-nonanedithiol (NDT, 95%), 11-mercaptoundecanoic acid (MUA, 95%), and sodium borohydride ($NaBH_4$, 99%) were purchased from Aldrich. Dicarboxylic acids of the type $H_2OC-(CH_2)_n-CO_2H$ included 1,6-hexanedicarboxylic acid (n = 6, HDA, 98%), 1,9-nonanedicarboxylic acid (n = 9, NDA, 97%), 1,10-decanedicarboxylic acid (n = 10, DDA, 99%), 1,11-undecanedicarboxylic acid (n = 11, UDA, 94%), and 1,14-tetradecanedicarboxylic acid (n = 14, TDA, 96%), which were purchased from Aldrich, and 1,12-dodecanedicarboxylic acid (n = 12, DDDA), 1,13-tridecanedicarboxylic acid (n = 13, TDDA, 97%), 1,16-hexadecanedicarboxylic acid (n = 16, HDDA, 97%), and 1,18-octadecanedicarboxylic acid (n = 18, ODDA), which were purchased from TCI America. Iodine (I_2, 100%) was purchased from Fisher. Solvents included hexane (99.9%) and toluene (99.8%) from Fisher and ethanol (99.9%) from Aldrich. Deuterated solvents included dimethyl sulfoxide (DMSO, 99.9%) and chloroform ($CDCl_3$, 99.9%) from Cambridge Isotope Laboratories. Water was purified with a Millipore Milli-Q water system.

Synthesis of Nanoparticles. Au−Ag alloy nanoparticles (core size = 3.0 ± 0.5 nm) capped with alkanethiolate (e.g., DT) monolayer shells were synthesized by the two-phase reduction of $AuCl_4^-$ and $AgBr_2^-$. We have recently reported detailed procedures[6] for the synthesis of composition-controlled Au−Ag alloy nanoparticles. Briefly, the synthesis was carried out by separately transferring $AgBr_2^-$ and $AuCl_4^-$ from the aqueous phase to the organic phase using TOABr as the phase-transfer agent. The subsequent reduction of the metal precursors by $NaBH_4$ led to DT-capped alloy nanoparticles. For example, for the synthesis of Au−Ag (1:4 molar ratio) nanoparticles,[6] 1.63×10^{-4} mol of $HAuCl_4$ was dissolved in 25 mL of water, and phase transfer was executed using 8.96×10^{-4} mol of TOABr in toluene (50 mL). Then, 6.83×10^{-4} mol of $AgNO_3$ was dissolved in 50 mL of water and added (dropwise) to an aqueous solution (50 mL) of KBr (7.43×10^{-3} mol, factor of 10 molar ratio) under vigorous stirring, and phase transfer was executed using 9.07×10^{-4} mol of TOABr in toluene (50 mL). The above two toluene phases, containing $AgBr_2^-$ and $AuCl_4^-$, were then combined and stirred for 30 min. Subsequently, 5.5×10^{-7} mol of decanethiol (DT) was added as a capping agent, and 6.50×10^{-3} mol of $NaBH_4$ (in 12 mL of water) was added (dropwise) as a reducing agent. The reaction mixture was stirred for 4 h, yielding decanethiolate-encapsulated Au−Ag (1:4 mole ratio) alloy nanoparticles in the toluene phase. The solvent was removed by evaporation, and the particles were suspended and washed three times using ethanol. The particles were then dried and dissolved in hexane.

Preparation of Thin-Film Assembly. The general preparation of the thin films involved immersion of substrates (e.g., glass) into a hexane solution of DT-capped Au_n-Ag_{100-n} nanoparticles (1.0 μM) and dicarboxylic acid [$HO_2C-(CH_2)_n-CO_2H$ (n = 6−18)] as a mediator or cross-linking agent at room temperature. The linker-to-nanoparticle (Au_n-Ag_{100-n}) ratio was 100:1. The substrates were immersed vertically to ensure that the film formed was free of powder deposition. After a controlled immersion time, the film-deposited substrates were removed and immediately rinsed thoroughly with hexane and dried by blowing with nitrogen before characterization.

Instrumentation and Measurements. *Transmission Electron Microscopy.* Transmission electron microscopy (TEM) was performed on a Hitachi H-7000 electron microscope (100 kV). Samples were prepared by drop-casting nanoparticles dissolved in hexane solution onto a carbon-coated copper grid sample holder and then allowing natural evaporation to proceed at room temperature. Thin films were made by immersion of carbon-coated copper grid sample holders into the assembly solution for a controlled time followed by rinsing with hexane.

UV−Visible Spectroscopy. UV−visible spectra were acquired with a single-beam HP 8453 spectrophotometer. The spectra were collected over the range of 200−1100 nm. Unless otherwise stated, the nanoparticle solutions were in hexane and the nanoparticle films were deposited on glass (microscope slide or cover glass).

X-ray Photoelectron Spectroscopy (XPS). XPS measurements were carried out using a Physical Electronics Quantum 2000 Scanning ESCA Microprobe. This system uses a focused monochromatic Al Kα X-ray (1486.7 eV) source for excitation and a spherical section analyzer. The percentages of individual elements were determined from the relative composition analysis of the peak areas of the bands based on corresponding sensitivity factors.

Fourier Transform Infrared (FTIR) Spectroscopy. FTIR spectra were acquired on a Nicolet 760 ESP FTIR spectrometer that was purged with boil-off from liquid N_2. The spectrometer was equipped with a liquid nitrogen-cooled HgCdTe detector. For transmission FTIR spectra, the nanoparticle film sample was mixed with KBr powder and ground into fine powders. The powders were pressed into a pallet at 15000 psi. For samples deposited as thin films on reflective surfaces, infrared reflectance spectroscopy (IRS) was used. A variable-angle reflectance device was used, and the incident beam was p-polarized light with a grazing angle of 82° with respect to the surface normal. A gold slide coated with octadecanethiolate-d_{37} monolayer was used as the IRS reference. Gold thin film on Cr-primed glass (Au/glass) was used as a substrate for the IRS measurements. IR spectra were collected over the range of 400−4000 cm^{-1}.

Nuclear Magnetic Resonance Spectroscopy. ^1H NMR spectra were collected at 360 MHz on a Bruker (AC) spectrometer. Deuterated DMSO and chloroform were used as solvents. Samples,

(33) Finklea, H. O. In *Electrochemistry*; Bard, A. J., Rubinstein, I., Eds.; Marcel Dekker: New York, 1996; Vol. 19, p 107.
(34) Poirier, G. E. *Chem. Rev.* **1997**, *97*, 1117.
(35) (a) Lin, S. Y.; Tsai, T. K.; Lin, C. M.; Chen, C. H.; Chan, Y. C.; Chen, H. W. *Langmuir* **2002**, *18*, 5473. (b) Choi, H. J.; Han, S. W.; Lee, S. J.; Kim, K. *J. Colloid Interface Sci.* **2003**, *264*, 458.
(36) (a) Tao, Y. T.; Lee, M. T.; Chang, S. C. *J. Am. Chem. Soc.* **1993**, *115*, 9547. (b) Tao, Y. T. *J. Am. Chem. Soc.* **1993**, *115*, 4350. (c) Tao, Y. T.; Hietpas, G. D.; Allara, D. L. *J. Am. Chem. Soc.* **1996**, *118*, 6724.

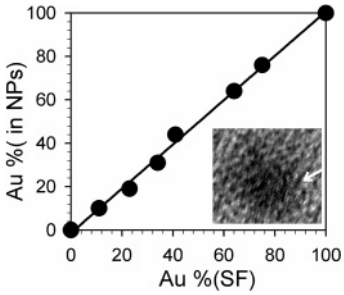

Figure 1. Relationship between the percentage of Au in the nanoparticles (in NPs) vs the percentage of Au in the synthetic feeding (SF) for Au_n-Ag_{100-n} (slope = 0.98, $r^2 = 0.99$). Inset: HRTEM image of a $Au_{23}-Ag_{77}$ nanoparticle.

sealed in a 5-mm-diameter NMR tube, were placed into the spinner turbine and inserted into the magnet by means of airlift. The rotation frequency was adjusted to 20 Hz. Temperature was maintained at 300 K during the experiments. The chemical shift of the solvent was used as a reference for the calibration.

Conductivity Measurements. Conductivity measurements were performed using an interdigitated microelectrode (IME) as the substrate for thin-film deposition. The IME has 310 pairs of gold electrodes on a glass substrate with a 5-μm width and a 5-μm spacing. The resistance measurement used a computer-interfaced multimeter (Extech). The temperature dependence was determined in a sealed glass tube purged with N_2 and immersed in a bath of ethanol mixed with dry ice.

Results and Discussion

The description and discussion of the results are divided into four sections. We first describe the composition and the morphology of the Au−Ag alloy nanoparticles and their thin-film assemblies. The optical and electrical properties of the thin-film assemblies are discussed in the second and third sections, respectively. In the last section, we discuss the interparticle reactivities and mechanistic insights for the dicarboxylate-mediated thin-film assembly of the alloy nanoparticles.

Composition and Morphology of Au−Ag Nanoparticles and Thin-Film Assemblies. We have recently shown[6] that the alloy composition of the Au−Ag nanoparticles, as determined by direct current plasma−atomic emission spectroscopy (DCP−AES), can be precisely controlled by manipulating the feed ratios of the two metal precursors in a modified two-phase protocol (Figure 1). The alloy nanoparticles are denoted as Au_n-Ag_{100-n}. It is important to note that the alloy nanoparticles are highly crystalline, as shown by the observation of the well-defined crystal facets in the HRTEM image for $Au_{23}-Ag_{77}$ (Figure 1 inset).

The thin film thus deposited appeared very uniform and displayed colors ranging from brown to purple depending on the alloy composition and the film thickness. Figure 2A shows a typical set of photos for the HDA-mediated thin-film assembly of $Au_{23}-Ag_{77}$ particles on glass substrates. The appearance of the thin film was quite comparable to that of films derived similarly for gold nanoparticles using other molecular mediators or linkers such as MUA and NDT.[20] The TEM examination showed network morphologies (Figure 2B) for a submonolayer assembly of $Au_{23}-Ag_{77}$ nanoparticles linked by HDA, formed on a carbon-coated copper grid after a short immersion time (15 min). In comparison with unlinked nanoparticles (prepared by casting DT-capped nanoparticles and evaporating the solvent, as described in a previous report[6]), the film displays features of small domains of ordered arrays that are branched into a network. In addition, the image clearly reveals particles with individually identifiable sizes and shapes. Such features were observed for films ranging from submonolayer to monolayer coverage. Because of the lack of large ordered domains, we were not able to definitively determine the interparticle spacing at this time. Further work on this aspect is needed, including SAXS measurements.[37]

On the basis of our studies of the thin-film assembly of molecularly mediated gold nanoparticles on different substrates,[20] we believe that the film formation involves an initial exchange between linkers and shell molecules, followed by precipitation of the cross-linked nanoparticles as a continuous thin film on a solid surface. This is a phenomenon observed for materials at the nanoscale. In some cases, the film growth can be described by Avrami's theoretical model known for crystallization and growth of macromolecules.[20b] In general, the adhesion for the nanoparticle assembly on the surface of a variety of substrates involves a combination of van der Waals and other interactions (e.g., hydrogen-bonding), the latter of which depends on the nature of the functional groups on the linker/shell molecules and the substrate. These interactions involve multiple binding sites because of the network structure of the linked nanoparticles. The film thickness is dependent on the solution concentrations of the

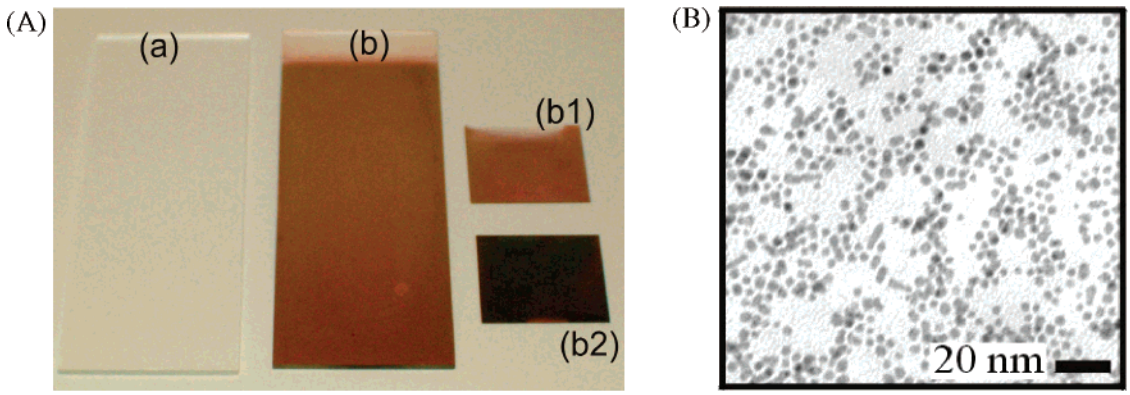

Figure 2. (A) Photos of the thin-film assemblies on a microscope glass slide: (a) bare glass, (b) HDA-mediated thin-film assembly of $Au_{23}-Ag_{77}$/glass. b1 and b2 show thinner or thicker films, respectively, formed on cover glass substrate. (B) TEM micrograph for a submonolayer of an HDA-linked assembly of $Au_{23}-Ag_{77}$ nanoparticles.

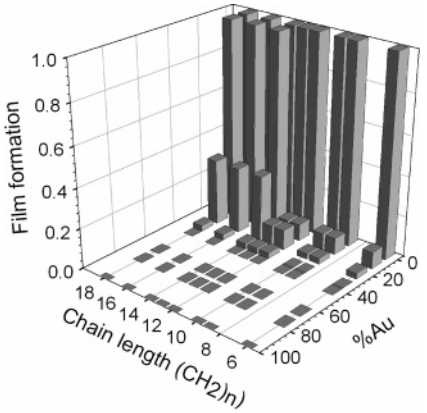

Figure 3. Comparison of thin-film formation vs the percentage of Au in the Au−Ag nanoparticles and chain length (number of CH_2 units) of the dicarboxylic acid. Linker-to-nanoparticle ratio = 10:1 for Ag and 100:1 for Au_n-Ag_{100-n}; $[Au_n-Ag_{100-n}] = 1.0\ \mu M$. The film formation is based on the measurement of the absorbance of the surface plasmon resonance band at its maximum (500−540 nm) in a defined immersion time, which is proportional to the relative speed of the thin-film formation.

nanoparticles, linker molecules, and assembly time. However, the reaction kinetics were also found to play an important role in the film formation, because rapid precipitation occurs when the concentrations are too high and film formation is insignificant when they are too low. In the present work, the thin-film assembly of Au−Ag nanoparticles is also found to be dependent on the composition of the alloy and the chain length of the mediator. The measurement of the absorbance of the surface plasmon resonance band at its maximum (500−540 nm) for the thin film formed on a glass substrate in a defined immersion time provides an effective means for assessing the relative thin-film formation. Figure 3 summarizes such a set of experimental observations for the thin-film formation of Au_n-Ag_{100-n} nanoparticles mediated by a series of dicarboxylic acids of different chain lengths *n* [$H_2OC-(CH_2)_n-CO_2H$]. It was measured by normalizing the data for each film formation to that for the fastest film formation (the maximum absorbance of the surface plasmon resonance band is ∼0.1) within a defined time length. The results are shown for thin-film formation as a function of the alloy composition (Au percentage) of the Au−Ag nanoparticles and the chain length *n* (i.e., number of CH_2 units) of the dicaboxylate linkers. First, clear indications for the formation of thin films were observed for Au_n-Ag_{100-n} nanoparticles with <35% Au. Nanoparticles of other compositions did not show any indication of thin-film formation even after a period of over 3 months. Second, the thin-film formation was much faster for nanoparticles with a low percentage of Au than for those with a high percentage of Au. Monometallic gold nanoparticles did not show any indication of thin-film assembly with the dicarboxylic acids. In contrast, monometallic silver nanoparticles exhibited very good thin-film assembly with the dicarboxylic acids. The presence of silver on the Au−Ag nanocrystal surface evidently plays an important role in the thin-film assembly. Third, the thin-film formation mediated by a long-chain dicarboxylic mediator was faster than that mediated by a shorter-chain mendiator. Clearly, the interparticle reactivities of exchange and cross-linking are dependent on both the alloy composition of the nanoparticles and the chain length of the mediator.

Although we have studied Au_n-Ag_{100-n} nanoparticles of different alloy compositions, this report focuses on detailed descriptions and discussions of the reactivities and properties for a representative alloy composition, i.e., $Au_{23}-Ag_{77}$ nanoparticles, unless stated otherwise.

Optical Properties. The surface plasmon (SP) resonance band of metal nanoparticles strongly depends on the size, shape, composition, and dielectric property of the nanoparticles and the local environment.[20,38] Figure 4 shows a representative set of UV−vis data to characterize the SP properties for HDA-mediated thin-film assembly of $Au_{23}-Ag_{77}$ nanoparticles on a glass substrate. The spectrum for a solution sample is included for comparison. In comparison to its solution counterpart (460 nm), the SP band for the HDA-mediated assembly of $Au_{23}-Ag_{77}$ nanoparticles showed a significant shift to longer wavelength (515 nm), which is characteristic of changes in interparticle spacing and properties of the dielectric medium. The intensity of the SP band increases with assembly time (Figure 4B), which is indicative of the growth of the film thickness as evidenced by the darkening of the brownish color of the film. This optical change is similar to that observed for gold nanoparticle assemblies mediated by MUA linker.[20]

In Figure 5, the red shift of the SP band from the spectrum for (b) DT-capped $Au_{23}-Ag_{77}$ nanoparticles in solution to that for (a) the HDA-linked $Au_{23}-Ag_{77}$ film reflects changes in the interparticle distance and the properties of the dielectric medium.[20,38] Importantly, the thin-film assembly of the Au−Ag nanoparticles is further found to be disassembled upon the introduction of ligands that can release the dicarboxylate linker molecules, demonstrating the integrity of the individual nanoparticles. For example, the thin-film assembly can be

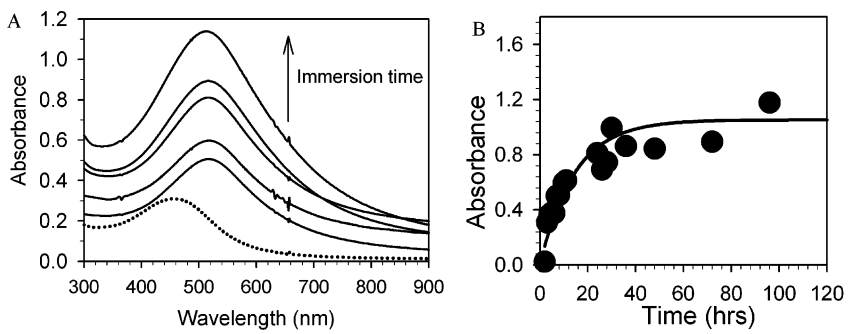

Figure 4. UV−vis data. (A) Spectral evolution as a function of assembly time (8, 10, 24, 72, and 120 h) (solid lines) for HDA-linked thin-film assembly of $Au_{23}-Ag_{77}$ nanoparticles and the nanoparticles in hexane solution (dotted line). (B) Plot of absorbance at 515 nm vs assembly time.

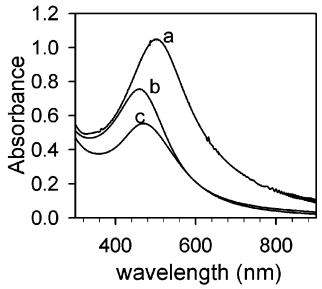

Figure 5. UV−vis spectra for (a) HDA-linked assembly of $Au_{23}-Ag_{77}$, (b) DT-capped $Au_{23}-Ag_{77}$ in hexane, and (c) the HDA-linked $Au_{23}-Ag_{77}$ film redissolved in 0.5 M hexylamine/hexane.

completely dispersed into a solution of 0.5 M hexylamine (in hexane). The SP band for the dissolved nanoparticles basically returned in wavelength from 502 nm for the assembled film to 460 nm as is characteristic of the $Au_{23}-Ag_{77}$ nanoparticles in the solution. The subtle difference in peak shape between the initial and redissolved nanoparticles is due to differences in solvent, capping agent, and concentration. The dissolution of the film in 0.5 M hexylamine (in hexane) implies that hexylamines displace dicarboxylates from the nanoparticle surface, leading to the disassembly of the film. Although the detailed mechanistic aspects of the replacement are not clear, we believe that the strong ion-pairing between $-NH_3^+$ and $-CO_2^-$ is partly responsible for the release of the dicarboxylates from the nanocrystal surfaces.

Electrical Properties. The electronic conductivity of nanoparticle assemblies is known to be dependent on core size and intercore distance.[20e,39] In a preliminary assessment of the electronic properties of our thin-film assemblies, the films were assembled on an interdigitated microelectrode (IME),[20c] and the resistance (R_Ω) was measured, which is related to the lateral electronic conductivity (σ) of the film by the relationship of $\sigma = (1/R_\Omega)(w/dL)$, where w is the gap width of the array electrodes, L is the length of the electrodes, and d is the film thickness. Figure 6 shows plots of $\ln(1/R_\Omega)$ as a function of reciprocal temperature ($1/T$) for thin-film assemblies of $Au_{23}-Ag_{77}$ nanoparticles that were derived from dicarboxylic acids of two different chain lengths (n = 14 and 16). In this comparison, the film thicknesses were ensured to be comparable, i.e., 147 layers for the case of n = 14 and 152 layers for the case of n = 16.

Assuming an electron-hopping type of electronic conductivity in the indicated temperature range,[20e] the analysis of the $\ln(1/R_\Omega)$ vs $1/T$ plots shows that the conductivity is dependent on the chain length of the linker molecules. The activation energy, E_a, was found to be 0.04 eV for n = 14 and 0.05 eV for n = 16. The E_a values are remarkably comparable to values reported for other films.[10,20e,39] For example, a value of 0.03 eV was found for films of NDT-linked gold nanoparticles of 5-nm size and 0.14 eV for those

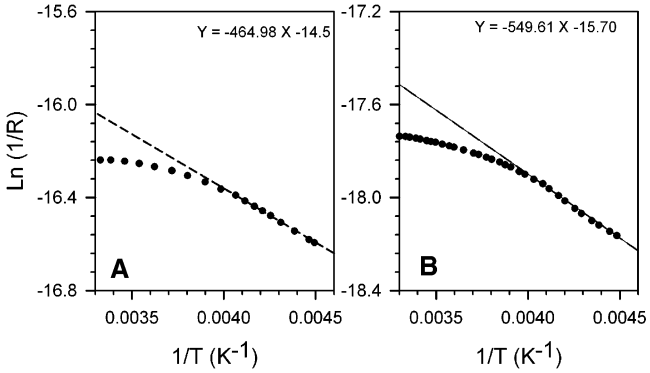

Figure 6. Plots of $\ln(1/R_\Omega)$ versus $1/T$ for thin-film assemblies of DT/$Au_{23}-Ag_{77}$ nanoparticles mediated by dicarboxylates of n = (A) 14 and (B) 16.

Table 1. Comparison of the Changes in Absorbance of the SP Band between HDA- and NDT-Linked Film Assemblies of DT/Au_{23}–Ag_{77} Nanoparticles on Glass and the Assembly Solutions (in Hexane) under Different Conditions

exptl atmosphere	abs for soln[a]	abs for film
	HDA−DT/$Au_{23}-Ag_{77}$	
O_2	0.25	0.73 (∼135 layers)
air	0.22	0.75 (∼139 layers)
Ar	0.72	0.65 (∼120 layers)
H_2	0.89	0.50 (∼92 layers)
	NDT−DT/Au_{23}–Ag_{77}	
O_2	0.20	0.52 (96 layers)
air	0.23	0.53 (98 layers)
Ar	0.21	0.49 (91 layers)
H_2	0.23	0.51 (95 layers)

[a] The data were obtained using the SP band absorbance data for solutions, which were normalized by dividing the data by the absorbance of the Au_{23}–Ag_{77} solution in the absence of linker (abs =1.00). Assembly time = 11 h. The numbers of layers in parentheses were estimated from the absorbance and the ϵ value.[21b]

of NDT-linked gold of 2-nm size.[20e] We believe that the comparability in conductivity might in fact reflect the operation of a similar electron-hopping mechanism.

Interparticle Reactivities. To probe whether silver−carboxylate bond formation at the silver sites is responsible for the interparticle binding chemistry, film formation was examined under several different oxidative and reductive conditions. These conditions were believed to manipulate the degree of surface silver oxidation during the ligand-exchange step. This concept was demonstrated by carrying out the thin-film assembly under different atmospheres, i.e., solutions that were saturated with different gases such as oxygen, hydrogen, argon, and air. The absorbance values of the SP band from films formed on glass and those from the assembly solution after a given period of time (11 h) were compared to assess the rate of film formation. Table 1 shows a representative set of data.

In Table 1, data from NDT-linked thin-film assemblies under identical conditions were included for comparison. In the NDT case, the silver−thiolate binding chemistry is in sharp contrast to the silver−carboxylate binding chemistry in the HDA case. There are several important findings. First, in comparison to the thin-film assembly under hydrogen, the HDA-linked thin-film assembly under oxygen atmosphere displayed a larger increase in absorbance of the SP band for the film and a larger decrease in absorbance for the assembly

(37) Maye, M. M.; Lim, I.-I. S.; Luo, J.; Rab, Z.; Rabinovich, D.; Liu, T.; Zhong, C. J. *J. Am. Chem. Soc.* **2005**, *127*, 1519.
(38) (a) Alvarez, M. M.; Khoury, J. T.; Schaaff, T. G.; Shafigullin, M. N.; Vezmar, I.; Whetten, R. L. *J. Phys. Chem. B* **1997**, *101*, 3706. (b) Link, S.; El-Sayed, M. A. *Int. Rev. Phys. Chem.* **2000**, *19*, 409.
(39) Terrill, R. H.; Postlethwaite, T. A.; Chen, C. H.; Poon, C. D.; Terzis, A.; Chen, A. D.; Hutchison, J. E.; Clark, M. R.; Wignall, G.; Londono, J. D.; Superfine, R.; Falvo, M.; Johnson, C. S.; Samulski, E. T.; Murray, R. W. *J. Am. Chem. Soc.* **1995**, *117*, 12537.

Table 2. Comparison of the Change in Absorbance of the SP Band in the Assembly Solution for HDA-Linked Assembly between Aged and Unaged Au_{23}–Ag_{77} Nanoparticles under Air and Hydrogen Atmospheres

exptl conditions	abs/soln[a]
aged in air	0.50
aged in H_2	0.96
unaged in air	0.56
unaged in H_2	0.86

[a] The data were obtained using the SP band absorbance data for solutions, which were normalized by dividing the data by the absorbance of the Au_{23}–Ag_{77} solution in the absence of linker (abs =1.00). Assembly time = 24 h.

solution within the same time frame (e.g., 11 h). The use of air or nitrogen to replace oxygen or argon, respectively, had similar effects on the absorbance changes, but to a lesser extent. This finding indicates that oxidizing conditions in the solution accelerate thin-film assembly, whereas reducing conditions impede thin-film assembly. Second, in contrast to the HDA assembly, the NDT assembly showed little dependence on the assembly atmosphere for both film and assembly solution after 11 h. This finding indicates that the formation of surface silver oxide as an intermediate step is likely an important component for the silver–carboxylate-based binding chemistry for the nanoparticle assembly. The oxidizing effect does not seem to be significant for the silver– or gold–thiolate binding chemistry. The presence of oxygen in the assembly solution might play a significant role in stabilizing the positively charged silver sites or promoting further oxidation during the ligand-exchange process. In contrast, the reducing effect of hydrogen could destabilize surface silver oxide formation, resulting in a slower ligand-exchange process. In another experiment using freshly synthesized Au–Ag nanoparticles, little film was observed for the HDA-linked assembly under hydrogen atmosphere even after 2 days, supporting the above assessment.

To understand the significance of surface silver oxide formation in the HDA-linked thin-film assembly of Au–Ag nanoparticles, we further studied the effect of aging the nanoparticles under ambient or oxygen atmosphere before assembly. The aging was carried out by purging a freshly synthesized nanoparticle solution with oxygen or leaving the nanoparticle solution for at least 1 week at ambient conditions. Table 2 shows a typical set of data comparing the change in absorbance of the SP band in the assembly solution for the HDA-linked assembly between aged and unaged Au_{23}–Ag_{77} nanoparticles under air and hydrogen atmospheres. It is evident that aging of the nanoparticles did not have much effect on the rate of assembly compared to the results on the effect of the atmosphere under which the assembly occurs. This finding is consistent with the results discussed above.

The surface composition of the Au–Ag nanoparticles before and after assembly was also analyzed using XPS. Table 3 shows a typical set of XPS data. There are several important findings. First, the close comparability of the surface compositions of silver and gold before and after assembly indicates that there is no phase change in the alloy composition and the two metals remain intact during the assembly process. Second, the oxygen composition before and after assembly shows a ~4-fold increase in percentage of oxygen for the HDA-linked nanoparticles, which is consistent with the ligand exchange in the HDA-mediated assembly. Third, there is a subtle decrease of the percentage of sulfur upon thin-film assembly, which is again consistent with ligand exchange in the HDA-mediated assembly, which leads to the replacement of a small fraction of thiolates by carboxylates.

Important information on the core–shell binding properties was provided by an analysis of the S 2p binding energy (BE) for decanethiolates on the nanocrystal surface and other surface species. A set of XPS spectra in the Au 4f, Ag 3d, and S 2p regions is shown in Figure 7. The binding energies for these peaks are listed in Table 4. The fact that both Au ($4f_{7/2}$ and $4f_{5/2}$) and Ag ($3d_{5/2}$ and $3d_{3/2}$) bands were identified[40] in the thin film supports the assembly of alloy nanoparticles, rather than a mixture of two monometallic nanoparticles, because we could detect only Ag for the HDA-mediated assembly if a mixture of DT/Au and DT/Ag nanoparticles was used. A close comparison of the binding energies for the Au 4f and Ag 3d bands (Figure 7A,B) before and after the thin-film assembly indicates a subtle increase (0.2 eV) for the assembled nanoparticles. This finding suggests that some of the surface atoms of the assembled nanoparticles (Ag and Au) carry more positive partial charges than for the as-synthesized nanoparticles. This is a result of the replacement of some of the DTs by HDAs. The increased partial positive charge for Ag is consistent with the fact that the Ag^+–CO_2^- bond is more ionic than the Ag–SR bond.[36c] We believe that some of the increased positive charges were likely distributed to the nanocrystal surface, leading to an increased positive charge on Au atoms, which explains the observation of a subtle increase of the binding energy for Au 4f bands.

A close examination of the relative ratio and binding energy (BE) of the S 2p doublet bands (Figure 7C) reveals additional information. The doublet feature is characteristic of sulfur from the thiolate species adsorbed on Au and Ag. Spectral deconvolution with a Lorentzian profile was applied to analyze the doublet bands. The fitting constraint is a doublet of peaks that have a width of ~0.95 ± 0.10 eV at one-half of the peak-height and a difference in binding energy of 1.2 eV between the $2p_{3/2}$ and $2p_{1/2}$ peaks. An important finding is that ratio of the $2p_{3/2}$ and $2p_{1/2}$ peaks for the as-synthesized Au–Ag nanoparticles is close to 2:1 expected for thiolates adsorbed on Au surface.[40] Interestingly, the deconvolution data for the assembled nanoparticles showed two sets of doublet (162.0 and 163.2 eV, 162.4 and 163.6

Table 3. XPS Data for DT/Au_{23}–Ag_{77} Nanoparticles before and after HDA-Linked Thin-Film Assembly

	elemental composition (%)				
sample	C 1s	O 1s	Ag 3d	Au 4f	S 2p
DT/Au_{23}–Ag_{77}	72.05 ± 0.65	2.05 ± 0.25	16.45 ± 0.25	4.55 ± 0.15	4.9 ± 0.1
HDA assembly of DT/Au_{23}–Ag_{77}	65.55 ± 0.15	9.05 ± 0.45	16.25 ± 0.25	4.65 ± 0.15	4.5 ± 0.1

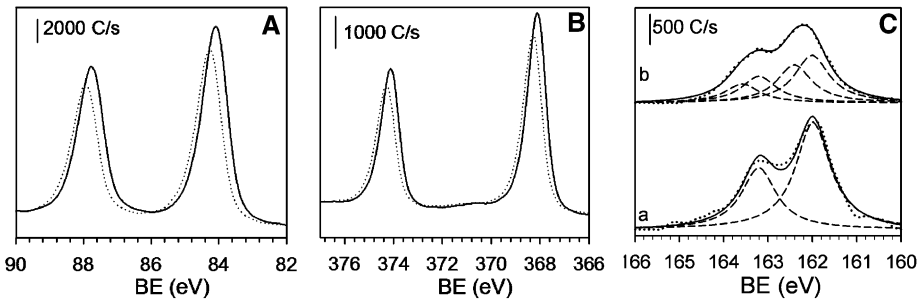

Figure 7. XPS spectra in the (A) Au 4f, (B) Ag 3d, and (C) S 2p regions for $Au_{23}-Ag_{77}$ nanoparticles. In A and B, the curves correspond to data obtained before (solid line) and after (dotted) HDA-linked thin-film assembly. In C, the spectra in the S 2p region obtained (a) before and (b) after assembly. The dotted line represents the experimental data, and the dashed and solid lines represent spectral deconvolution results in C. The C 1s peak (285.0 eV) serves as an internal reference.

Table 4. XPS Peak Positions (BE/eV) for $Au_{23}-Ag_{77}$ Nanoparticles before and after HDA-Linked Thin-Film Assembly[a]

	Au		Ag		S	
sample	$4f_{7/2}$	$4f_{5/2}$	$3d_{5/2}$	$3d_{3/2}$	$2p_{3/2}$	$2p_{1/2}$
$DT/Au_{23}-Ag_{77}$	84.0	87.6	368.0	374.0	162.0	163.2
HDA assembly of $DT/Au_{23}-Ag_{77}$	84.2	88.0	368.2	374.2	162.0	163.2

[a] C 1s peak (285.0 eV) serves as an internal reference.

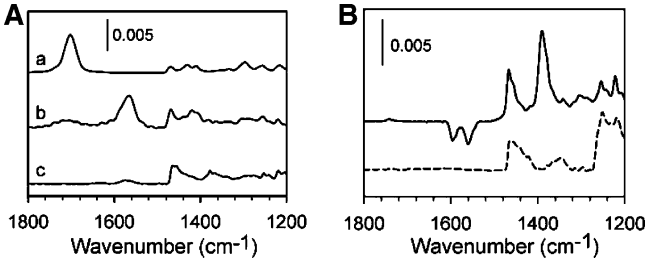

Figure 8. (A) FTIR spectra of (b) HDA-linked thin-film assembly of $Au_{23}-Ag_{77}$ nanoparticles. Spectra of (a) neat HDA and (c) DT-capped $Au_{23}-Ag_{77}$ nanoparticles are included for comparison. Samples were made into KBr pellets. (B) IRS spectra of thin-film assembly of $Au_{23}-Ag_{77}$ nanoparticles on a gold-coated glass slide (solid line, HDA-linked; dashed line, NDT-linked).

eV) in which the lower-BE component is predominant (65.5%). The difference of the binding energy for these two sets likely reflects a subtle difference in partial negative charges on sulfur due to the environmental effect on the distribution of the surface positive charges, in agreement with the increase of the partial positive charge on the nanocrystal surface as discussed previously.

FTIR characterization of the HDA-linked thin-film assembly of $Au_{23}-Ag_{77}$ nanoparticles provided useful information for assessing the structures of the capping/linking materials. Both transmission-mode FTIR spectra of the thin-film samples made with KBr powders and reflection-mode spectra (IRS) of the thin films deposited on a gold-coated glass slide were acquired (Figure 8). A gold-coated glass slide with an octadecanethiolate-d_{37} monolayer was used as the IRS reference.

In the transmission-mode spectra (Figure 8A), the spectrum of an HDA-linked thin-film assembly of $Au_{23}-Ag_{77}$ nanoparticles (b) is compared with spectra for control samples such as HDA and $DT/Au_{23-}Ag_{77}$ nanoparticles (a, c). The detection of an asymmetric carboxylate stretching band [$\nu_a(COO^-)$] at ~1564 cm^{-1} in the HDA-linked thin-film assembly of $Au_{23}-Ag_{77}$ nanoparticles (b), in contrast to the detection of $\nu(CO_2H)$ at 1710 cm^{-1} for HDA (a), indicates that the exchange and cross-linking processes involved carboxylate−Ag linkages. We note that the presence of a small band at ~1568 cm^{-1} in the spectrum for the as-synthesized $Au_{23}-Ag_{77}$ nanoparticles (c) could be attributed to advantageous hydrocarbon species arising from the possible oxidation of silver sites during thorough rinsing in sample preparation. It has previously been shown that the carboxylic acid group for self-assembled monolayers of alkanoic acids on a silver surface is in the form of caboxylate with a bidentate binding to Ag. This binding was supported by the detection of the $\nu_s(CO_2^-)$ band at ~1400 cm^{-1} and absence of the $\nu_a(CO_2^-)$ at 1500−1600 cm^{-1}.[41] In the reflection IRS data (Figure 8B), the results indicate the presence of both $\nu_s(CO_2^-)$ at 1391 cm^{-1} and $\nu_a(CO_2^-)$ at 1576 cm^{-1}. We note that the spectrum for the HDA assembly revealed an unusual negative absorbance feature on both the high- and low-wavenumber sides of the $\nu_a(CO_2^-)$ band at 1576 cm^{-1}. This distinctive feature is reproducible. We believe that it likely reflects an electronic effect of the film. A similar "anomalous" negative-going peak was previously observed on the high-wavenumber side for CO adsorption on carbon-supported Pt nanoparticles deposited on gold substrate,[42] which are often observed in aggregated metal nanoparticle films associated with their complex dielectric behavior[42a] or complex optical effects (e.g., refractive index effect).[42b] We note that such a negative-going peak is absent in the IRS spectra of the NDT-linked thin-film assembly of $Au_{23}-Ag_{77}$ nanoparticles. This finding serves as a further confirmation of carboxylate−Ag^+ binding in the case of the HDA-linked thin-film assembly, in contrast to the thiolate−gold binding in the case of the NDT-linked thin-film assembly. Although further IRS characterization of the thin film is underway, our results point to a monodentate binding of the dicarboxylate on the silver component of the alloy nanoparticles. This finding is in contrast to the bidentate binding of the carboxylic acid groups in self-assembled monolayers of alkanoic acids on silver surface.[41d]

(40) Castner, D. G.; Hinds, K.; Grainger, D. W. *Langmuir* **1996**, *12*, 5083.

(41) (a) Seo, Y. U.; Lee, S. J.; Kim, K. *J. Phys. Chem. B* **2004**, *108*, 4000. (b) Han, H. S.; Han, S. W.; Kim, C. H.; Kim, K. *Langmuir* **2000**, *16*, 1149. (c) Lee, S. J.; Han, S. W.; Choi, H. J.; Kim, K. *J. Phys. Chem. B* **2002**, *106*, 2892. (d) Lee, S. J.; Han, S. W.; Yoon, M.; Kim, K. *Vib. Spectrosc.* **2000**, *24*, 265.

(42) (a) Park, S.; Weaver, M. J. *J. Phys. Chem. B* **2002**, *106*, 8667. (b) Mielczarski, E.; Duval, Y. B.; Mielczarski, J. A. *J. Phys. Chem. B* **2002**, *106*, 11985.

Table 5. ^{1}H NMR Chemical Shifts and Integrated Areas for the Diagnostic Proton Peaks for Products Released from Several Molecularly Mediated Thin-Film Assemblies of Au−Ag Nanoparticles

	$-CH_3$		$-S-S-CH_2-CH_2$		$-S-S-CH_2-$		$-OOC-CH_2-CH_2$		$-OOC-CH_2-$	
sample	ppm	area	ppm	area	ppm	area	ppm	area	ppm	area
DT−Au−Ag[a]	0.89	3.00	1.68	1.41	2.69	1.45	−		−	−
HDA/DT−Au−Ag[a]	0.89	3.00	1.68	1.19	2.69	1.63	−		−	
MUA/DT−Au−Ag[a]	0.89	3.00	1.68		2.69	1.26	2.29	0.47	4.12	0.53
HDA/DT−Au−Ag[b]	0.81	3.00	1.54	−	2.56	1.11	−	−	2.14	0.34

[a] I_2 treatment. [b] I_2 and HCl treatment.

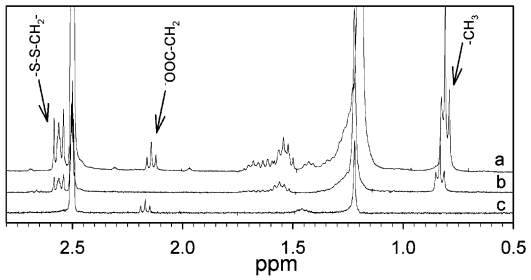

Figure 9. (a) ^{1}H NMR spectra of products released from HDA-linked assembly of $Au_{23}-Ag_{77}$ nanopartilces. Spectra of (b) neat DT and (c) neat HDA samples are included for comparison.

One of the most important quantitative assessments of the interparticle exchanging and linking properties for the dicarboxylic acid linked Au−Ag nanoparticle film formation was provided by NMR characterization. Figure 9 shows a representative ^{1}H NMR spectrum for a sample derived from the reaction of HDA-linked $Au_{23}-Ag_{77}$ nanoparticles with I_2 and HCl in DMSO-d_6 (a). Spectra for DT (b) and HDA (c) treated similarly are included for comparison. The experiments involved desorption of the shell molecules by treatment with either I_2 alone or I_2 plus subsequent addition of concentrated hydrochloric acid (HCl). In the case of treatment with I_2 alone, ^{1}H NMR spectra obtained from products showed 1.7 ($-S-S-CH_2-CH_2-$) and 2.7 ($S-S-CH_2-$) ppm peaks for MUA-linked $Au_{33}-Ag_{77}$ nanoparticles, which were very similar to those observed for $DT-Au_{33}-Ag_{77}$ nanoparticles. In addition, another set of peaks was observed at 2.3 ($HOOC-CH_2-CH_2-$) and 4.1 ($HOOC-CH_2-CH_2-$) ppm (Table 5), which is consistent with our previous study of the degree of exchange for MUA-linked monometallic gold nanoparticles.[16] However, for HDA-linked $Au_{33}-Ag_{77}$ nanoparticles, ^{1}H NMR spectra obtained from the products did not display the peaks characteristic of HDA (i.e., $HOOC-CH_2-CH_2-$ and/or $HOOC-CH_2-CH_2-$). This is likely due to the difficulty of breaking the silver−carboxylate bond. In the case of treatment of I_2 plus HCl, the dicarboxylates can be released by forming dicarboxylic acids. This experiment involved the addition of deuterated dimethyl sulfoxide (DMSO-d_6) (∼5 mL), iodine (I_2)[43] (∼10 mg), and concentrated hydrochloric acid (∼50 μL) into a flask containing the nanoparticle film assembly (on the walls of flask). The flask contents were stirred for 3 h, after which the reaction released both capping DT and linking carboxylate ligands (e.g., HDA) from the nanoparticle surface as disulfide and dicarboxylic acid molecules, respectively. This reaction was qualitatively evidenced by the complete disappearance of the brown/black color of the nanoparticle film, which is likely an indication of the conversion of the nanoparticles into their metal ions. The chemical shifts and the integrated peak areas are included in Table 5. The released products from the HDA-linked $Au_{23}-Ag_{77}$ nanoparticles showed peaks at 2.14 ppm characteristic of $-OOC-CH_2-$ in HDA. The 0.81 ppm peak is characteristic of $-CH_3$ in DT, indicating the presence of DT in the HDA-linked assembly. From the ratio of the peak at 2.14 ppm to that at 0.81 ppm, the degree for the DT-HDA exchange was estimated, yielding a value of 16% of DTs per particle being displaced by HDAs.

The above results were further compared with NMR analysis of the released products from the MUA-linked assembly of DT-capped $Au_{23}-Ag_{77}$ nanopartilces treated only with I_2,[42] to release the capping thiolate as dithiols, in chloroform (Table 5). The released products showed peaks at 4.12 ppm characteristic of $-CH_2-COOH$ in MUA and at 0.89 ppm characteristic of $-CH_3$ in DT. We noted a shift of the $-CH_3$ triplet in the ^{1}H NMR spectrum from the HDA-interlinked alloy nanoparticles (0.81 ppm) compared to the DT-capped alloy nanoparticles (0.89 ppm). The reason for this shift is not clear, but we speculate that it could be due to the difference in solution environment. The degree of exchange estimated from the relative peak ratio yielded a value of 21% of DTs per particle being displaced by MUA. The fact that this value is greater than that for the HDA-linked Au−Ag assembly (21%) and smaller than that for the MUA-exchanged solution system (38%[43]) and MUA-linked assembly system (46%[16]) supports the conclusion that the dicarboxylic acid mediated assembly of Au−Ag nanoparticles occurs via carboxylate linkages at silver sites, whereas carboxylic acid functionalized thiol mediated assembly occurs via thiolate linkages on both gold and silver sites on the nanoparticle surface.

Conclusion

In conclusion, the interparticle linkage of dicarboxylate acids at selective silver sites of Au−Ag nanoparticles has been demonstrated as a new strategy for molecularly mediated thin-film assembly of binary metal nanoparticles. The interparticle chemistry involves the carboxylate−silver and the chain−chain interaction in the alkyl shell structures. The manipulation of the core composition and linker chain length could provide new opportunities for exploiting the binary nanoparticle-structured sensing and catalytic properties. The results from controlling the oxidative or reductive conditions reveal that the oxidation of Ag to Ag^+ on the alloy nanocrystal surface played an important role in the selective ligand exchange and interparticle linkage by dicarboxylic acids. The formation of the thin-film assembly is dependent

(43) Templeton, A. C.; Hostetler, M. J.; Kraft, C. T.; Murray, R. W. *J. Am. Chem. Soc.* **1998**, *120*, 1906.

on both the alloy composition of the Au−Ag nanoparticles and the chain length of the dicarboxylic acids. The degree for an HDA−DT/Au−Ag exchanging and linking system is determined to be 16% of DTs per Au−Ag particle being displaced by HDAs. It is concluded that the HDA-mediated assembly of Au−Ag nanoparticles occurs via $-CO_2^- - Ag^+$ linkages at silver sites forming a mediator (HDA)−template (DT) nanostructure. Although an in-depth investigation is underway to probe the detailed surface composition and binding chemistry of the alloy nanocrystals, the interesting optical and electronic properties exhibited by the nanostructured thin films have important implications on the exploration of binary nanoparticle-structured materials for sensing and catalytic applications where fine-tuning of either the binary nanocrystal cores or the bifunctional interparticle structures is desired.

Acknowledgment. Financial support of this work from National Science Foundation (Grants CHE 0316322 and 0349040) is gratefully acknowledged. We thank M. H. Engelhard and Y. Lin (Environmental and Molecular Sciences Laboratory at Pacific Northwest National Laboratory) for XPS measurements, H. H. Eichelberger (Department of Biology, SUNY-Binghamton) for assistance in TEM measurements, and H. R. Naslund (Department of Geological Sciences, SUNY-Binghamton) for assistance in DCP-AES analysis.

CM0519479